Chapter 3

Ultrafast Electron Crystallography: Methodology and Apparatus

Introduction

The apparatus of ultrafast electron crystallography (UEC) was built for the studies of condensed matter and surface assemblies (*1, 2*), on the basis of the experiences accumulated through the construction of the first three generations for gas-phase molecular studies in our group (*3, 4*). Conceptually, the UEC technique uses the similar scheme of laser excitation (pump) and electron probing, in which the optical initiation marks the zero of time. With the specimen mounted inside the chamber, its diffraction pattern is digitally recorded. By varying the delay time between the arrival of the optical and electron pulses on the surface of the specimen, diffraction snapshots at different times are obtained; the diffraction patterns contain information about the structural evolution, as a function of time, of the material under study. The analysis of diffraction feature changes provides the temporal profiles for certain physical processes, as described in Ch. 2. Finally, structural dynamics and an overall physical picture are obtained through the correlation between these processes.

The UEC apparatus can be operated in the reflection or transmission detection mode. Their experimental configurations are basically the same, except for a small difference in that for transmission, an additional vertical sample holder is used to support the thin specimens; the electron beam penetrates through a sample instead of being scattered from a surface. This chapter briefly describes the parts that form the apparatus and discusses about several topics in the experimental consideration. Details for the construction of the instrument may be found in Ref. 2. A further development implementing the scheme of pulse front tilting (*5*) was made by Dr. Peter Baum. Its concept for resolving the temporal mismatch between the optical and electron pulses on the specimen (thus improving the temporal resolution of UEC) is also summarized.

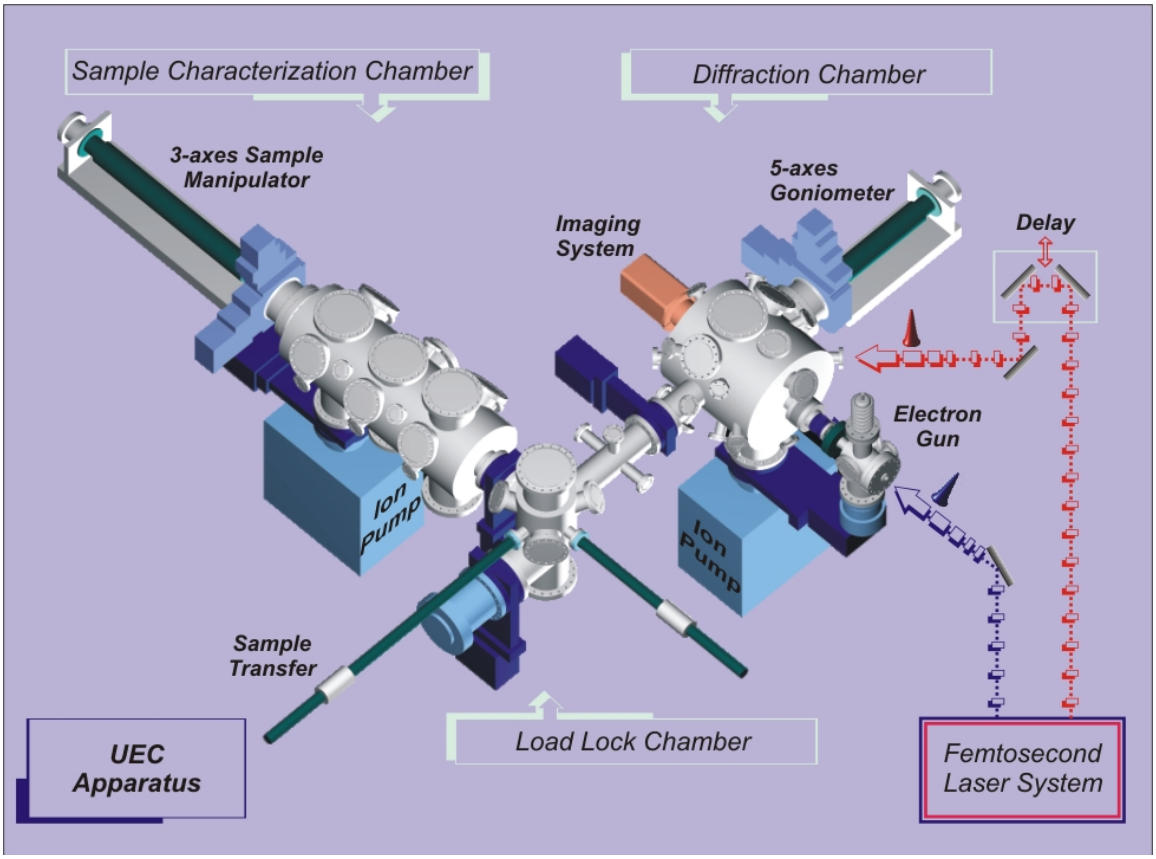

Fig. 1. UEC apparatus. Shown are the three UHV chambers and the two laser beams from the femtosecond laser system for optical excitation and electron generation.

Apparatus of UEC

The UEC apparatus consists of a femtosecond laser system for generation of the electron probe and optical initiating pulses; an assembly of ultrahigh vacuum (UHV) chambers for diffraction, load lock (sample handling) and characterization; an electron gun system in a high vacuum chamber; and a charged-couple device (CCD) camera assembly for pattern recording (Fig. 1). The UHV environment is necessary for the surfaces and interfacial assemblies that are sensitive to pressure as a result of their easy deterioration caused by the bombardment or coverage of gas molecules. Manual and pressurized gate valves (dark blue modules in Fig. 1) were installed for the separation

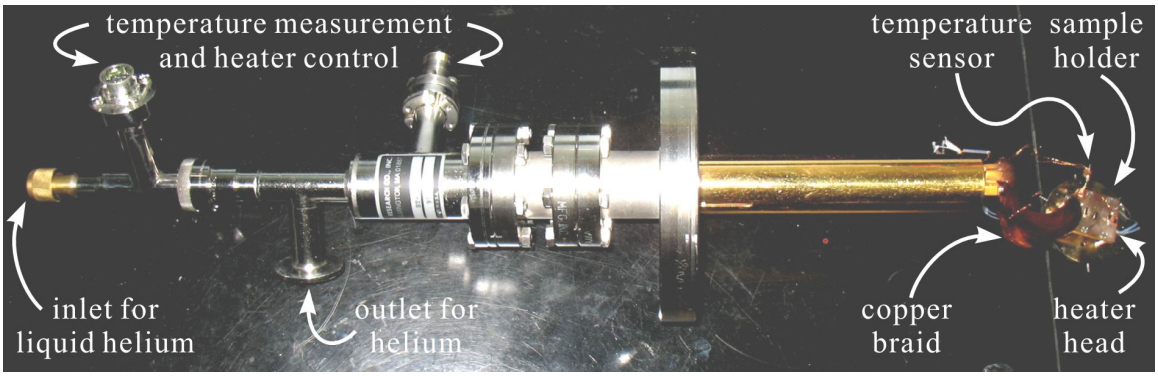

Fig. 2. The cryostat for low-temperature experiments. The copper braid cooled by the flow of liquid helium conducts thermal energy away from the sample holder. A heater is also available for temperature adjustment.

(isolation) of chambers when necessary. The different pressures between the electron gun, diffraction chamber and the CCD camera are maintained through differential pumping.

For position control of the samples, a high precision goniometer (from Transfer Engineering) with 3 degrees of freedom in translation and 2 axes of rotation was installed and housed inside the diffraction chamber. These translations and rotations are manipulated through a computerized interface, allowing for precise alignment of the specimens (supported on a sample holder mounted onto the goniometer), the measurement of rocking curves by changing the incidence angle (θ), and the access of the zone axes at different azimuthal angles (ϕ). The translational precision is 10 μm and the angular precision is 0.005°. Tubes for the flow of liquid nitrogen were connected from the bottom of the goniometer inside the diffraction chamber and intended for low-temperature experiments; the minimum temperature that may be reached by this method is ~100 K. For experiments that require an even lower temperature, the sample holder on the goniometer is coupled to a UHV cryostat (ST-400, Janis Research) that is connected from one side of the diffraction chamber and cooled by liquid helium (Fig. 2).

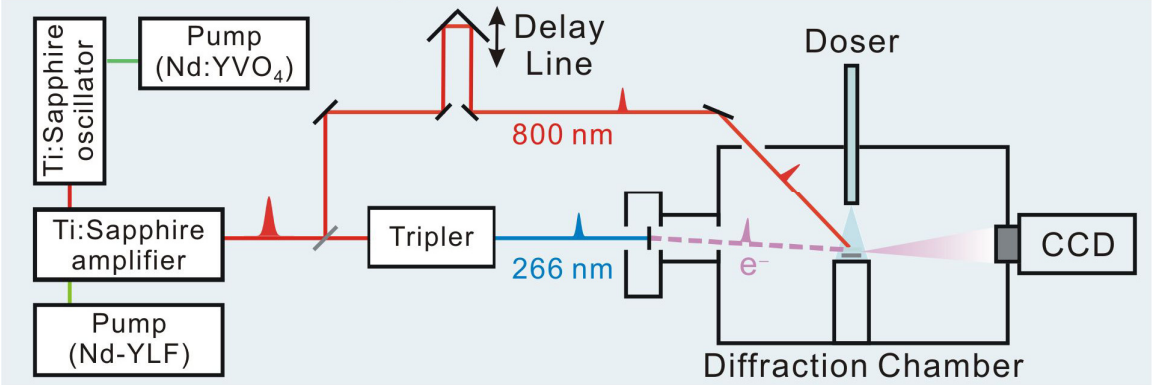

Fig. 3. Schematic of the femtosecond laser system and its integration into the UEC apparatus. The arrangement of the beam paths is specifically for experiments that consider the specimen excitation to be achieved by near-infrared 800-nm light pulses. A capillary doser is connected to the top of the chamber for studies of molecular assembly.

A temperature of ≤20 K is readily achieved without too fast helium consumption. As for experiments that require a temperature higher than the room temperature, the wires installed under the goniometer head can heat the sample holder (up to ~500 K) through the adjustment of the electric current; its influence on the electron beam direction is small and, therefore, does not interfere with the recording of diffraction images.

The femtosecond laser system consists of an oscillator, an amplifier, and two pump lasers (Fig. 3). The mode-locked Ti:sapphire oscillator (Tsunami, Spectra-Physics) is pumped by a continuous-wave, diode-pumped Nd:YVO_4 laser (Millennia Vs, Spectra-Physics) with an average power of 5 W at 532 nm. The output of the oscillator is femtosecond laser pulses centered at 800 nm, with a repetition rate of 80 MHz and a pulse energy of 8 nJ. These pulses are amplified by a Ti:sapphire amplifier (Spitfire, Spectra-Physics) pumped by a diode-pumped, Q-switched Nd:YLF laser (Evolution-30, Spectra-Physics) whose repetition rate is 1 kHz and pulse energy is >20 mJ centered at 527 nm. The output of the amplifier is femtosecond pulses centered at 800 nm (1.55 eV),

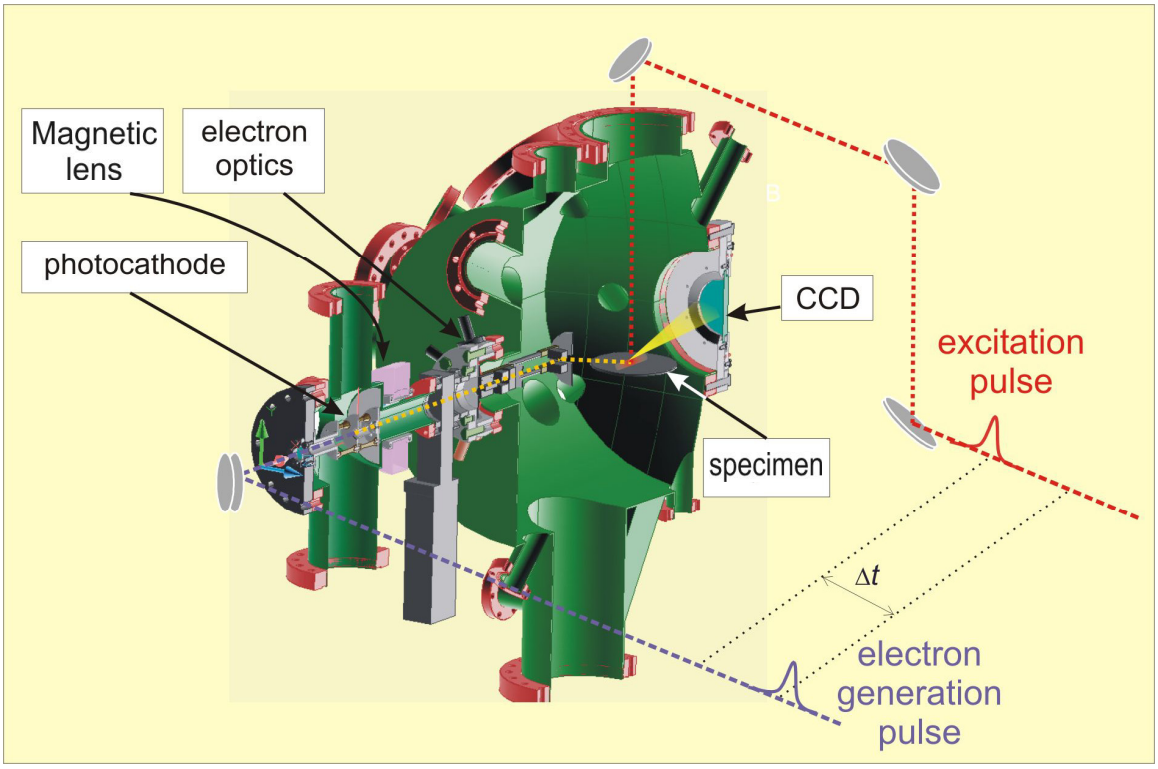

Fig. 4. A cross-sectional view of the electron gun and diffraction chambers, with the paths of the optical excitation and electron generation beams and the CCD camera.

with a full width at half maximum (FWHM) in time equal to ~120 fs and a pulse energy of 2 mJ at 1 kHz.

For experiments that use 800-nm light to excite the specimens, a beam splitter is placed to separate the main beam into two arms (Fig. 3). The path of the stronger beam for excitation contains a movable delay line for the variation of time, which is controlled through a computerized interface; optical pulses are directed and loosely focused at an angle of 60° from the sample's surface normal to initiate the "temperature jump." The energy of the pump pulse can be varied by using neutral density filters. Such a configuration is referred to as the original excitation scheme. The frequency of the weaker beam is tripled via third harmonic generation with the use of a commercial tripler

(TP-1A, U-Oplaz Technologies). This ultraviolet beam at 266 nm (4.65 eV) is used to generate ultrashort electron pulses through the photoelectric effect (see below). In regard to experiments with 266-nm excitation, the beam splitter is placed after the whole 800-nm beam from the amplifier passes through the tripler, in order to separate a stronger arm for initiation and a weaker one for electron generation; the rest of the beam paths remain the same as the original excitation scheme at 800 nm.

Electron pulses are generated by the 266-nm beam back-illuminating the photocathode (Fig. 4), which is made of a thin silver film (~45 nm in thickness) deposited by the vapor deposition method on a sapphire window that is enclosed by a close-fitting groove at the end of the stainless steel cathode set; see Figs. 3-4 and 3-5 in Ref. 4 for illustration of the electron gun assembly. Before deposition of the silver film, the edge of the sapphire window is first glued to the groove rim with the use of conductive silver paint for the window's immobility and good electric contact. The cathode set is connected to a high voltage supply (FC60N2, Glassman High Voltage) through a vacuum feedthrough, and the anode is grounded to the whole chamber system.

In our experiments, the typical pulse energy of the 266-nm beam for the electron generation is on the order of sub-microjoule or below. It is focused on the photocathode, and the number of photoemitted electrons in a pulse is in the range of several hundred to few thousand (adjusted by varying the intensity of the ultraviolet beam with the use of neutral density filters). The purpose of limiting the electron number is to maintain a temporal width of several hundred femtoseconds to few picoseconds that is suitable for the detection of ultrafast structural dynamics (*6*). The photoemitted electrons are accelerated by a voltage of 30 kV in 3 mm, resulting in a de Broglie wavelength of ~0.07 Å. The electron pulses are focused by a magnetic lens and directed onto the

specimen after passing through a series of apertures and electrostatic deflection plates. The incidence angle of electrons is typically below 5°. Without hitting any object, the direct beam has a diameter (spatial FWHM) of ~200 μm (about 4 to 5 pixels) on the CCD screen, which becomes a time-independent contribution to the width of diffraction. The resulting average (current) flux of electrons is relatively small, on the order of 0.1–5 pA/mm^2 depending on the probing geometry. Therefore, no electron damage, modification, or charging of the specimens is observed for most experiments.

The CCD assembly (Fig. 2.6 in Ref. 2) has a low noise level and contains an image intensifier (V5181U-06, Hamamatsu), which enables single-electron detection. The camera (Princeton Instruments PI-SCX:1300/W, Roper Scientific) records 16-bit digital images through a computerized interface, with an intensity range from 0 to 65535 (= 2^{16}–1). The largest image range has 1340 pixels in the horizontal direction and 1300 pixels in the vertical; the measured pixel size is 44.94±0.25 μm in both directions. With a camera length (from the specimen to the phosphor screen) of ~16.8 cm, each pixel represents a scattering angle of 0.268 mrad, or 0.0240 Å^{-1} in the reciprocal space according to the definition of $s = (4\pi/\lambda)\sin(\theta/2)$. Therefore, with the help of curve fitting, the resolution of our apparatus reaches <0.01 mrad, i.e., few percent of a pixel or equivalent quantities; one example may be seen in Fig. 3b of Ch. 5. To block the undiffracted electrons (the direct beam) from reaching the phosphor screen and saturating the image intensity, a grounded, movable copper tube that serves as the beam trap is used during the recording of diffraction patterns.

The Scheme of Pulse Front Tilting

The most important factor that limits the temporal resolution of UEC, particularly

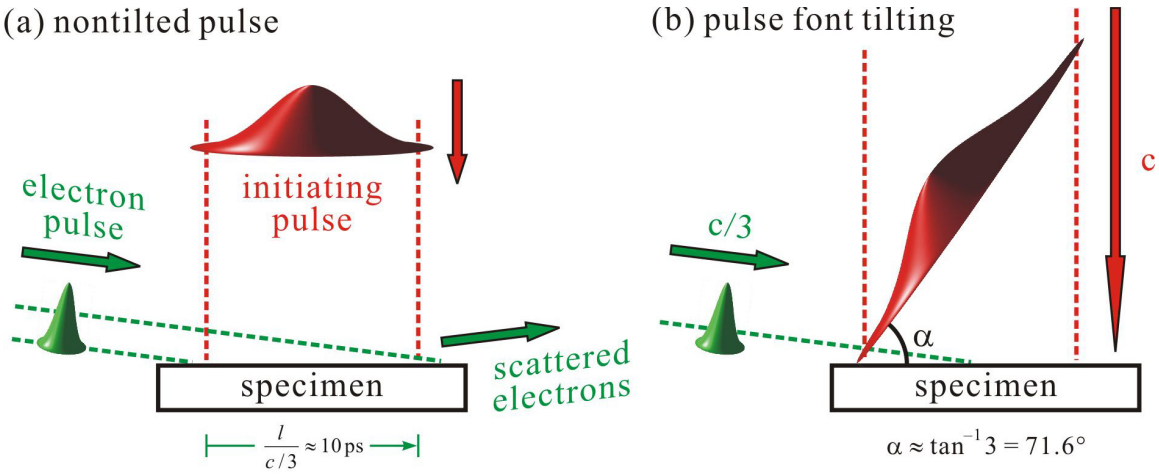

Fig. 5. (a) Mismatch between the arrival times of the nontilted initiating and electron pulses. The resulting temporal resolution is on the order of 10 ps. (b) The scheme of pulse front tilting. The extent of the pulse tilt is solely determined by the ratio of the speed of light to that of electrons.

in reflection experiments, is the mismatch between the optical initiating and electron probe pulses in the interaction region on the specimen. Even if the two pulses have femtosecond temporal widths, given the fact that electrons graze at a small incidence angle and probe the photoexcited region with a longitudinal dimension (l) on the order of 1 mm, the mismatch between the arrival times of the optical and electron pulses would be on the order of 10 ps for 30-keV electrons, whose velocity is 1/3 the speed of light (c) (Fig. 5a). Improving the temporal resolution in this excitation scheme requires reduction of the interaction region along the electron propagation direction, typically by limiting the useful sample region (see Ch. 4 and Ref. *7*). However, a natural consequence of this method is a substantial decrease of diffraction intensity in a given exposure time; unavoidable prolonged experiments may lead to other undesirable issues such as the long-term instability and sample deterioration.

The scheme of pulse front tilting can be implemented to solve the aforementioned temporal mismatch (*5*). As shown in Fig. 5b, the intensity front of the initiating pulse needs to be tilted by an angle of $\alpha \approx 72°$ to have the synchrony of the two pulses' arrival at every point of the interaction region on the specimen, because the ratio of the traveling speed of light to that of 30-keV electrons is ~3. Experimentally, a grating is used as the diffractive element for 800-nm light to introduce the angular dispersion and, concurrently, the traveling path difference necessary for pulse tilting. In addition, a spherical mirror is placed after the grating to gather the different spectral components originated and then dispersed from the same part of the spatial profile to coincide at the same corresponding point on the specimen; this method is optical imaging and effectively reconstructs the femtosecond optical pulse according to the energy–time uncertainty relation. The resulting reduction in time spread was confirmed to be better than 25 fold (*5*).

In Ch. 6, the application of the pulse tilting scheme proves to be critical to the resolution of ultrafast structural dynamics on the femtosecond time scale. The number of electrons per pulse is reduced to as low as ~500 in that study to minimize the space-charge effect (*6*) and, at the same time, maintain a reasonable duration for the experiments. With such a low flux, the electron pulse width of 322 ± 128 fs has been measured *in situ* at a streaking speed of 140 ± 2 fs/pixel (*8*). Although the overall temporal resolution is determined by convolution of the involved optical and electron pulses with any residual spread from pulse tilting, its improvement to ~400 fs is far better than the 20-ps spread estimated from the sample dimension of ~2 mm probed in the electron propagation direction. The pulse tilting scheme is also applied to the studies reported in Chs. 5, 7 and 8 and in Ref. *9*. Particularly for the latter two cases, the much improved temporal resolution is critical to the new discoveries.

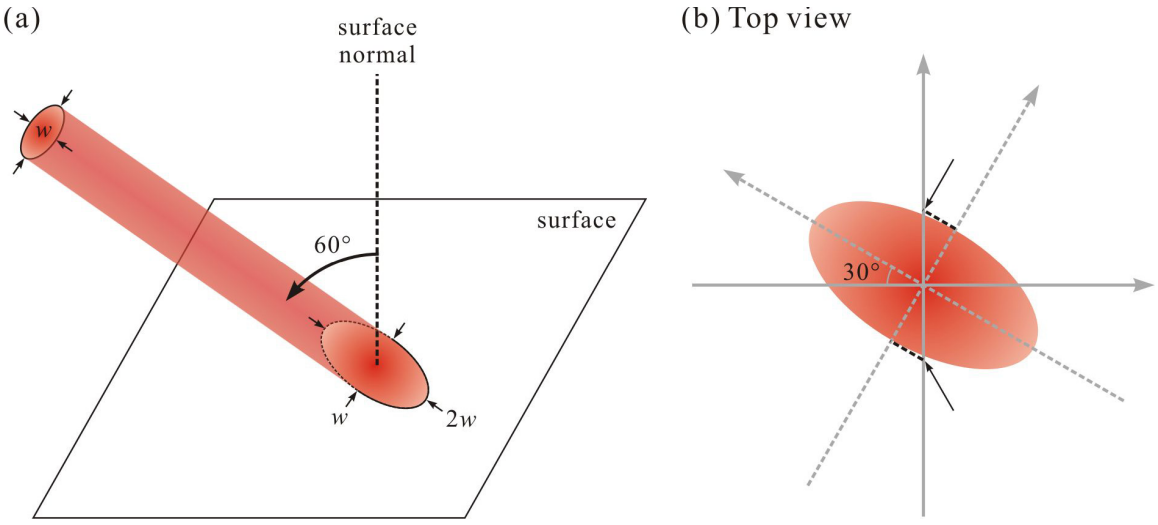

Fig. 6. The original excitation scheme and measurement of the FWHM. (a) The loosely focused optical beam impinges on the specimen at a specific incidence angle. (b) The width measurement determines the distance between the points indicates by the black arrows, which is $w/\cos 30°$ from the trigonometric relationship.

Experimental Consideration in UEC

A. Concerning Initiating Pulses and Optical Excitation

The first important thing to consider about the initiating pulse is the photon energy. Because ultrafast change of a specimen is initiated by photoexcitation in UEC, dynamics studies can only be made for materials that absorb the initiating pulses, whether the absorption is achieved through a one-photon process or through a multi-photon one. Thus, metallic materials and semiconductors with a band gap smaller than 4.65 eV may be investigated using the current laser system; the following chapters give examples for different types of substance. For insulating materials, although energetically possible, simultaneous absorption of two 266-nm photons for photoexcitation would be difficult to achieve due to the weak ultraviolet beam. Two other issues that may also restrict the UEC study of an insulator are the accompanying photoemission (which can affect the electron

beam path and probing) and surface charging (as a result of poor electric conduction).

The next important thing is the laser fluence on the specimen. Assuming that the beam profile is of a Gaussian form and its projection on the surface is circular, the peak fluence at the center is $F(r=0) = E_0 \cdot 4\ln 2/(\pi w^2)$, where E_0 is the integrated pulse energy and w is the spatial FWHM. To define the average fluence (F_{avg}) for such a beam, we consider the illuminated area to be 2 times the FWHM range, which gives $F_{avg} = 2E_0/(\pi w^2)$ to be smaller than the peak value, $F(r=0)$, but larger than half of it. This estimation is reasonable because the electron probed region (a stripe of 200 μm by few millimeters extending in the electron propagation direction) is intended to be narrower than and coincide with the intense part of the laser footprint in the horizontal direction. Therefore, the task of the estimation of fluence becomes measurement of the FWHM of the laser footprint.

The original excitation scheme produces an elliptical illuminated region on the specimen, as shown in Fig. 6. In the width measurement, the rod part of a needle was used as a blade to block the passing of the laser beam toward a photodiode, by which the intensity was recorded. According to the top view illustrated in Fig. 6b, the edge of the rod moved in the vertical direction, first intercepting with the beam from the bottom (indicated by the lower black arrow) and then totally blocking it (indicated by the upper black arrow); the rod diameter was larger than the FWHM of the beam. Thus, the recorded intensity curve was in the form of an error function, whose derivative was Gaussian with a FWHM equal to $w/\cos 30°$ (Fig. 6b). A typical value for w is 0.726 mm, and hence the corresponding temporal resolution is about 7 ps.

In the scheme of pulse front tilting, the initiating pulses impinge perpendicularly on the specimen, and the horizontal and vertical widths of the stretched elliptical footprint

were measured with the help of an auxiliary camera. During the measurement, the laser intensity was attenuated such that the peak fluence on the surface appeared to be just saturated in the screenshot captured by the auxiliary camera. The horizontal and vertical intensity profiles of the footprint were fitted to determine the (scaled) widths. Real FWHM values were obtained by multiplying the widths on the screen with the conversion factor (i.e., the ratio of a length in reality to its appearance in the screenshot), through the help of an object whose size was known. The common FWHM region used is 0.24 mm by 3 mm, which is large enough to make the electron probed region match with the higher fluence part after appropriate alignment (see below).

B. Concerning Electron Pulses and Probing

The important properties of an electron pulse include the number of electrons, its temporal width, and the energy and angular spread. The energy uncertainty is on the order of 10 V, given the output steadiness of the high voltage supply (<0.02% of rated voltage, 60 keV) and the excess energy above the work function of silver (tenths of a volt at most). A crude estimation of the electrons' angular spread in a pulse is given by the ratio of the initial size of photoemitted electrons (restricted by a pinhole of 150 μm) to the distance to reach the magnetic lens (~5 cm), or by the ratio of the pulse diameter on the CCD screen (~200 μm) to the traveling distance of electrons from the magnetic lens (67 cm), which is on the order of 0.1 to 1 mrad. Moreover, the spatial width of the electron beam also contains a small contribution from the little random jitter in the electron propagation direction around the average one. These factors consequently affect the coherence length seen by the electrons (Ch. 2).

Below the saturation level, the total intensity (above the noise level) recorded by the CCD camera is linearly dependent on the number of electrons that reach the phosphor

screen, at a given voltage for the image intensifier. Hence, the average electron number per pulse can be obtained by recording many single-pulse images, fitting the profiles to extract their total intensities, widths and positions, and dividing the intensity values by a conversion factor. This factor was previously obtained by counting the total intensity of each single-electron or few-electron event recorded in (at least) hundreds of images without magnetic lens focusing, and fitting the histogram of intensity to the Poisson distribution. The electron-generating 266-nm beam needed to be strongly attenuated such that only several electrons were generated in a pulse, with clear angular separation to make the counting process easier.

The relationship between the electron density in a pulse and its temporal width has been established by performing the streaking experiment (*1, 8*). Typically, for an increment of a thousand electrons per pulse, the width is increased by ≥1 ps. Thus, the major limitation of UEC's temporal resolution is the mismatch between the electron and optical pulses, and its solution by using the scheme of pulse front tilting was described earlier. During the experiments, diffraction patterns without laser excitation are recorded for the characterization of the specimens, and their differences are examined to see if the effect of electron charging, damage or modification exists as a result of constant electron bombardment. Our experiences show that the pulsed electron probing and existence of the bulk part of metallic or semiconducting samples (attached to the holder by conductive copper tape) greatly reduce the chance to encounter these undesirable issues. In contract, the surface morphology that contains sharp tips can be problematic because they may act as photoemitting sources or charge accumulation points, especially with laser excitation.

C. Aligning the Footprints of the Optical and Electron Beams

The major difficulty for the alignment of the interaction region is that the electron

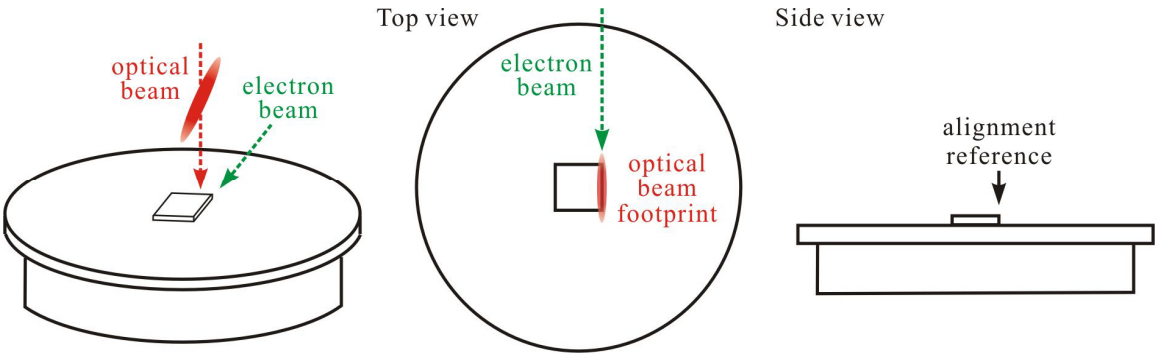

Fig. 7. Schematic for preliminary alignment of the optical and electron pulses. The edge of a substrate (e.g., sapphire) serves as the guideline.

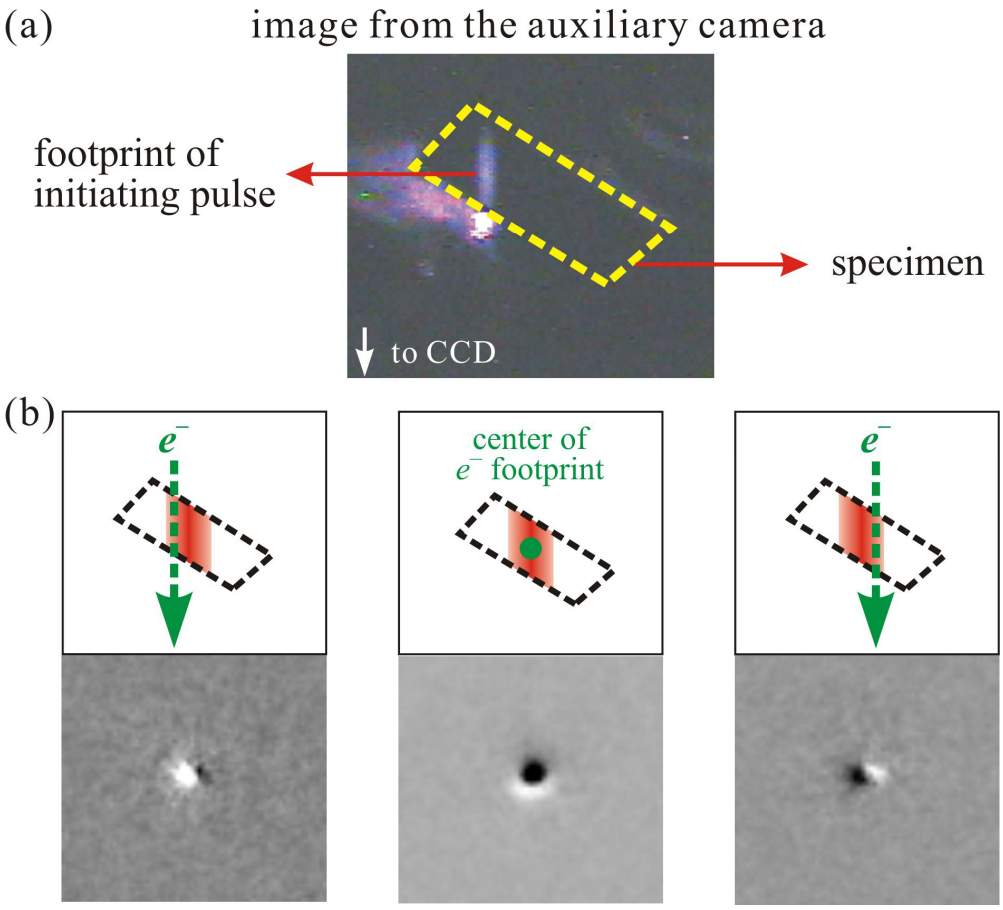

Fig. 8. Fine adjustment for the overlap of the laser and electron footprints. (a) An image taken by the auxiliary camera shows the specimen and the laser footprint. (b) Slight differences in the footprint overlap (upper panels) lead to different results in the diffraction difference images (lower panels).

beam footprint on the specimen is not visible. A method that utilized the tip of a stainless steel needle to intercept with the electron beam path was developed for the original excitation scheme (*2*). However, the alignment can be achieved by another method, with the use of a substrate that has straight and clear edges (e.g., 0.5-mm thick sapphire) and an auxiliary camera to monitor the substrate and the laser footprint (Fig. 7). For preliminary alignment, the substrate is rotated azimuthally such that one of its edges is approximately parallel to the electron path; the height of the goniometer is adjusted so that the electron beam can be blocked by the substrate but not by the sample holder. By moving the goniometer horizontally and monitoring the electron pulses in the CCD images, the edge can serve as a visual guideline for the electron beam path. The laser footprint is directed to match with the edge in the screenshot of the auxiliary camera when the electron beam is half-blocked.

For accurate alignment, the horizontal deflection voltage for electrons is to be adjusted. In the original excitation scheme, a small change of a few volts may be necessary for the observation of largest diffraction difference (referenced to the negative time frame) at positive delay times, which signifies a well-defined interaction region. In the case of the pulse tilting scheme, due to the comparable widths of the laser and electron footprints used, an imperfect alignment on the specimen in the horizontal direction may lead to horizontal asymmetry in the diffraction difference. An example is provided in Fig. 8, which shows the diffraction difference images obtained from a gallium arsenide sample with different overlaps of the footprints. This phenomenon can be related to both the small change in the Bragg condition and electron refraction because of the expanded lattice at positive times and the corresponding tilt of the surface normal for the wing parts of the optical excitation (Fig. 8b, left and right). With regard to the

vertical alignment, the height of the specimen is slightly adjusted to obtain the largest diffraction difference. If the sample has a dimension of ~1 to 3 mm, such an adjustment is expected to be achieved easily.

References:

1. C.-Y. Ruan, F. Vigliotti, V. A. Lobastov, S. Chen, A. H. Zewail, *Proc. Natl. Acad. Sci. USA* **101**, 1123 (2004).
2. S. Chen, Ph.D. thesis, California Institute of Technology (2007).
3. J. C. Williamson, Ph.D. thesis, California Institute of Technology (1998).
4. R. Srinivasan, Ph.D. thesis, California Institute of Technology (2005).
5. P. Baum, A. H. Zewail, *Proc. Natl. Acad. Sci. USA* **103**, 16105 (2006).
6. A. Gahlmann, S. T. Park, A. H. Zewail, *Phys. Chem. Chem. Phys.* **10**, 2894 (2008).
7. F. Vigliotti, S. Chen, C.-Y. Ruan, V. A. Lobastov, A. H. Zewail, *Angew. Chem. Int. Ed.* **43**, 2705 (2004).
8. V. A. Lobastov *et al.*, in *Ultrafast optics IV,* F. Krausz, G. Korn, P. Corkum, I. A. Walmsley, Eds., vol. 95 of *Springer series in optical sciences* (Springer, New York, 2004), pp. 419-435.
9. F. Carbone, P. Baum, P. Rudolf, A. H. Zewail, *Phys. Rev. Lett.* **100**, 035501 (2008).